A composition dependent energy scale and the determination of the cosmic ray primary mass in the ankle region

A.D. Supanitsky [a],*, A. Etchegoyen [b], D. Melo [b], F. Sanchez [b]

[a] Instituto de Astronomía y Física del Espacio (IAFE, CONICET-UBA), Buenos Aires, Argentina
[b] Instituto de Tecnologías en Detección y Astropartículas (CNEA, CONICET, UNSAM), Centro Atómico Constituyentes, San Martin, Buenos Aires, Argentina

ABSTRACT

At present there are still several open questions about the origin of the ultra high energy cosmic rays. However, great progress in this area has been made in recent years due to the data collected by the present generation of ground based detectors like the Pierre Auger Observatory and Telescope Array. In particular, it is believed that the study of the composition of the cosmic rays as a function of energy can play a fundamental role for the understanding of the origin of the cosmic rays.

The observatories belonging to this generation are composed of arrays of surface detectors and fluorescence telescopes. The duty cycle of the fluorescence telescopes is ∼10% in contrast with the ∼100% of the surface detectors. Therefore, the energy calibration of the events observed by the surface detectors is performed by using a calibration curve obtained from a set of high quality events observed in coincidence by both types of detectors. The advantage of this method is that the reconstructed energy of the events observed by the surface detectors becomes almost independent of simulations of the showers because just a small part of the reconstructed energy (the missing energy), obtained from the fluorescence telescopes, comes from simulations. However, the calibration curve obtained in this way depends on the composition of the cosmic rays, which can introduce biases in composition analyses when parameters with a strong dependence on primary energy are considered. In this work we develop an analytical method to study these effects. We consider AMIGA (Auger Muons and Infill for the Ground Array), the low energy extension of the Pierre Auger Observatory corresponding to the surface detectors, to illustrate the use of the method. In particular, we study the biases introduced by an energy calibration dependent on composition on the determination of the mean value of the number of muons, at a given distance to the showers axis, which is one of the parameters most sensitive to primary mass and has an almost linear dependence with primary energy.

© 2015 Elsevier B.V. All rights reserved.

1. Introduction

The cosmic ray energy spectrum extends over more than eleven orders of magnitude in energy (from below ∼10^9 eV to above ∼10^{20} eV). It can be approximated by a broken power law with four spectral features: the knee at a few 10^{15} eV [1–5], the ankle at ∼4×10^{18} eV [6–12], the cutoff or suppression at ∼3×10^{19} eV [9–12], and a second knee at ∼10^{17} eV, recently reported by the KASCADE-Grande Collaboration [13].

Several experimental techniques are used for the observation of the cosmic rays, depending on the energy range under consideration. In particular, the direct observation of the primary particles is possible up to energies of the order of ∼10^{15} eV. For larger energies the study of cosmic rays is done by observing the atmospheric air showers that they generate as a consequence of their interactions with air molecules in the atmosphere. There are two classes of ground-based detectors, surface detectors and fluorescence telescopes. The surface detectors observe the lateral distribution of the showers by sampling the secondary particles that reach the Earth's surface, whereas the fluorescence telescopes observe the fluorescence and Cherenkov photons generated, during the longitudinal development of the showers, as a result of the interaction of the secondary charged particles with the air molecules [14–17].

Despite great experimental effort done in the last years the origin of the cosmic rays is still unknown. The observations used to study their origin comprise: the energy spectrum, the distribution of the arrival directions, and the composition profile [18,19].

Certainly, the detailed study of the composition as a function of energy is of great importance to unveil the origin of the cosmic rays

at all energies (see Ref. [20] for a review on composition). In particular, it is believed that the composition information is crucial to find the transition between the galactic and extragalactic components of the cosmic rays (see for instance Ref. [21]) and to elucidate the origin of the suppression at the highest energies [22]. This feature of the spectrum could originate as a result of the propagation of the cosmic rays in the intergalactic medium, or by the end of the efficiency of the extragalactic sources to accelerate particles at the highest energies, or by a combination of both effects.

At the highest energies ($E \gtrsim 10^{15}$ eV), the composition of the cosmic rays is studied by using different observable parameters obtained from shower measurements which are very sensitive to the primary mass. The parameters most sensitive to primary mass are the atmospheric depth at which the maximum development of the showers is reached, which can be reconstructed from the fluorescence telescope data, and the muon content of the showers or a parameter closely related to it, which can be obtained from dedicated muon detectors (see for instance Ref. [23]).

The fluorescence light emitted during the shower development is proportional to the deposited energy. A fraction of these photons is detected by the fluorescence telescopes, making possible the reconstruction of the longitudinal profiles which yields an estimator of the energy of the primary particle. The energy reconstructed in this way is largely independent of simulations, just a small correction is done, by using simulations of the showers, which corresponds to the so-called invisible energy [24,25]. In contrast, the energy calibration of surface detectors alone has to be done by using detailed simulations of the showers and the detectors. The use of simulated showers introduces large systematic uncertainties because the hadronic interactions at the energies of the cosmic rays are unknown. Then, the models used for shower simulation extrapolate low energy data taken from accelerator experiments by several orders of magnitude in order to reach the energy of the cosmic rays. Note that, at present, the hadronic interaction models are being updated in order to reproduce the Large Hadron Collider data, which reaches up to cosmic ray energies of the order of $\sim 2 \times 10^{16}$ eV ($E_{cm} = 7$ TeV) [26–33].

The duty cycle of the fluorescence telescopes is $\sim$10% and that of the surface detectors is $\sim$100%. Therefore, in order to have a large duty cycle and an energy calibration almost independent of simulations, the present generation of cosmic ray observatories, the Pierre Auger Observatory in the southern hemisphere and Telescope Array in the northern hemisphere, combine both techniques. The energy scale of the surface detectors is obtained by using a parameter which is in general the interpolated signal at a given distance to the shower axis. The calibration curve that relates this surface parameter with the primary energy, reconstructed from the fluorescence telescope, is obtained experimentally from a subset of high quality events observed in coincidence by both types of detectors [11,12].

Therefore, if the surface parameter used as an energy estimator depends on primary type, the energy scale depends on the composition of the cosmic rays. The use of this energy scale in composition analyses introduces biases that can be important when the parameters used to infer the primary mass have a strong dependence on primary energy (see Ref. [34] for a first study).

In this work we study the effects of using an energy scale dependent on composition in mass composition analyses. For that purpose we develop a dedicated analytical method. We consider the AMIGA project [35] to illustrate in a simplified but realistic way the use of the method. The parameter sensitive to the primary mass is the number of muons at 600 m from the shower axis [36,37], which depends almost linearly with primary energy. Therefore, composition analyses based on this parameter are supposed to be quite affected by the use of a composition dependent calibration curve.

It is worth mentioning that many surface parameters like S_b [34], the risetime of the signals in surface detectors [38,39], the slope of the lateral distribution function [38,40], the curvature ratio of the shower front [39,41], etc. were proposed and sometimes used in composition analyses. The composition analyses that make use of these parameters together with a calibration curve dependent on composition are affected by the effect studied in this work for the case of the number of muons in the context of AMIGA. Each particular case involving different mass sensitive parameters and energy calibration methods has to be analyzed in detail in order to estimate the importance of the biases introduced by this practice.

2. Numerical approach

2.1. Simulations

The simulations used in this work are the ones generated for the studies done in Ref. [36], they correspond to AMIGA. AMIGA will consist in a triangular grid of 750 m spacing composed by pairs of detectors, a water-Cherenkov tank and a 30 m^2 muon counter buried underground. The energy region under consideration goes from $10^{17.6}$ eV up to $10^{18.5}$ eV.

The atmospheric air showers used in Ref. [36] to produce the simulated data were generated by using AIRES [42] with QGSJET-II-03 [43] as the high energy hadronic interaction model. The showers were simulated with fixed energies from $\log(E/eV) = 17.6$ to $\log(E/eV) = 18.5$ in steps of $\Delta \log(E/eV) = 0.1$. In this work just proton and iron primaries at 30° zenith angle are considered. For each primary energy and primary type a set 100 showers were generated.

The muon counters are segmented in 192 scintillation strips. Part of the light generated by a charged particle that goes through a given strip is collected by a wavelength shifter fiber optic and transported to a multi-anode photomultiplier. The electronics has an independent channel for each strip which gives a digital one as output for each muon pulse. Note that more than one muon arriving in a time interval corresponding to the width of a muon pulse is counted as one. That is called pile-up effect.

As described in Ref. [36], a simplified simulation of the muon counters is performed. Muon counters of 100% of efficiency buried underground at 2.5 m depth, which corresponds to a muon energy threshold of $\sim$0.82 GeV, are considered. The pile-up effect is also included in the simulations.

From the data taken by the Cherenkov detectors the lateral distribution function of the signal, the impact point, and the arrival direction of the showers are reconstructed. While the muon lateral distribution function is reconstructed from the data taken by the muon detectors, following the method developed in Ref. [36]. Note that the reconstruction method includes a correction for the pile-up effect.

The parameter used as energy estimator, considered in this work, corresponds to the interpolated signal collected by the water-Cherenkov detectors at 600 m from the shower axis, S, and the parameter sensitive to primary mass corresponds to the interpolated number of muons at 600 m from the shower axis, N_μ [44]. Note that the signal S is in units of VEM (vertical equivalent muon), which corresponds to the average signal deposited by a vertical muon that crosses the tank by its center [45]. Also note that N_μ is the total number of muons in an area of 30 m^2 for showers at $\theta = 30°$, therefore, it has no units.

The AMIGA muon detectors were designed for zenith angles from 0° to 45°. Therefore, we consider here showers of 30° because it is the median of the zenith angle distribution. The parameter N_μ for showers of different zenith angles can be transformed to 30° by using the corresponding muon attenuation curve [46].
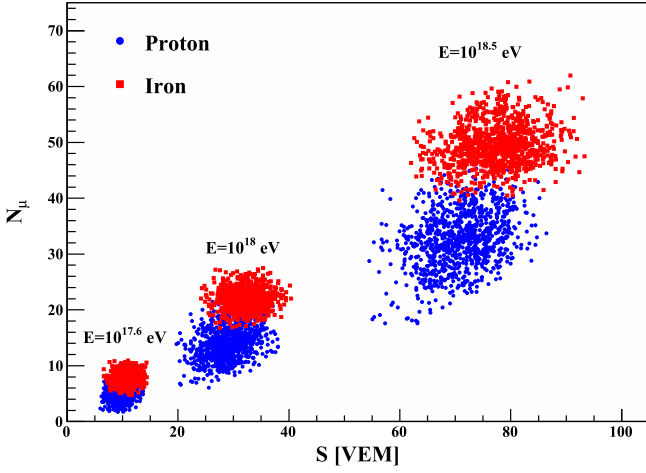
Fig. 1. N_μ versus S for $E = 10^{17.6}$, 10^{18}, and $10^{18.5}$ eV corresponding to proton and iron primaries of $30°$ of zenith angle. The high energy hadronic interaction model used is QGSJET-II-03.

Fig. 1 shows N_μ versus S for proton and iron primaries for three different values of primary energy.

The particle density at a given distance to the shower axis for the different types of particles of the showers presents shower to shower fluctuations. The corresponding distribution functions present asymmetric tails. However, the fluctuations introduced by the detectors and the effects of the reconstruction methods make a Gaussian function a good approximation of these distribution functions. Therefore, the combined distribution function of N_μ and S, given the primary energy and the primary type, can be approximated by a two-dimensional Gaussian function which is written as,

$$
P(N_\mu, S|E, A) = \frac{1}{2\pi\, \sigma[N_\mu]\, \sigma[S]\, \sqrt{1 - \rho^2}}
$$
$$
\times \exp\left[-\frac{1}{2(1 - \rho^2)} \left(\frac{(N_\mu - \langle N_\mu\rangle)^2}{\sigma^2[N_\mu]} + \frac{(S - \langle S\rangle)^2}{\sigma^2[S]} \right.\right.
$$
$$
\left.\left. -2\rho \times \frac{(N_\mu - \langle N_\mu\rangle)\ (S - \langle S\rangle)}{\sigma[N_\mu]\ \sigma[S]} \right) \right], \tag{1}
$$

where $(\langle N_\mu\rangle, \sigma[N_\mu])$ and $(\langle S\rangle, \sigma[S])$ are the mean value and the standard deviation of N_μ and S, respectively. The correlation ρ is given by,

$$
\rho = \frac{\mathrm{cov}(N_\mu, S)}{\sigma[N_\mu]\ \sigma[S]}, \tag{2}
$$

where $\mathrm{cov}(N_\mu, S)$ is the covariance between N_μ and S. Note that $\langle N_\mu\rangle$, $\langle S\rangle$, $\sigma[N_\mu]$, $\sigma[S]$, and ρ are functions of primary energy (E) and primary type (A).

The parameters $(\langle N_\mu\rangle, \sigma[N_\mu])$ and $(\langle S\rangle, \sigma[S])$ for each primary energy and primary type are obtained by fitting the corresponding one dimensional distributions with one dimensional Gaussian functions. The correlation ρ is obtained from the sample covariance and sample variances corresponding to each parameter (see Eq. (2)). Fig. 2 shows the one dimensional Gaussian fits to the proton and iron distributions of N_μ (top panel) and S (bottom panel) for two values of primary energy: $E = 10^{17.6}$ eV and $10^{18.5}$ eV. It can be seen from the figure that the Gaussian fits are a good description of the distribution functions.

In order to obtain an analytical representation of $P(N_\mu, S|E, A)$ the logarithm of the mean value as a function of the logarithm of primary energy and the standard deviation as a function of the logarithm of the primary energy, for each primary type and for each parameter (N_μ and S), are fitted. A linear function is used in
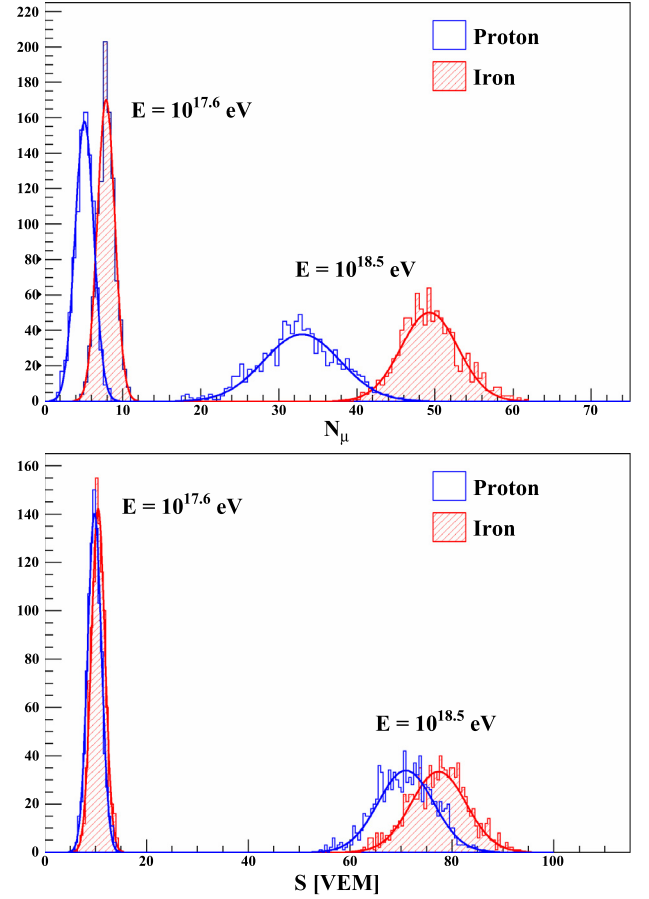

Fig. 2. One dimensional Gaussian fits to the proton and iron distributions of N_μ (top panel) and S (bottom panel). The primary energies considered are: $E = 10^{17.6}$ eV and $10^{18.5}$ eV.

all cases except the one corresponding to $\sigma[N_\mu]$, for which a better fit is obtained with a quadratic function. Also, the logarithm of the correlation as a function of the logarithm of primary energy is fitted with a linear function for both types of primaries considered.

The top panel of Fig. 3 shows the mean value of S as a function of the logarithm of primary energy for proton and iron primaries. Also shown are the fitted points (the error bars are included but they are smaller than the markers). The difference between these two curves is nearly constant, it increases from $\sim 9\%$ to $\sim 11\%$ in the energy range considered. The bottom panel of Fig. 3 shows the relative error of S which is given by, $\epsilon[S] = \sigma[S]/\langle S\rangle$. As expected, it decreases with primary energy for both primaries and it is smaller for iron nuclei in the whole energy range.

There are experimental evidences about a deficit on the number of muons in simulated showers [47]. As mentioned before, the hadronic interactions at the highest energies are unknown. As a consequence, models that extrapolate low energy data, obtained in accelerator experiments, to the energy of the cosmic rays are used. The signal in a water Cherenkov detector is the sum of the electromagnetic (due mainly to electrons, positrons, and gammas) and the muonic components. If the number of muons is larger than the one predicted by QGSJET-II-03, then S should be more sensitive to the primary mass. Therefore, in order to consider more general cases, the difference between the mean value of S for iron and proton primaries can be increased artificially. For that purpose let us introduce the parameter δ ($\delta \geqslant 0$) such that,

$$
\langle S\rangle(E, pr, \delta) = (1 - \delta) \times \langle S\rangle(E, pr),
$$
$$
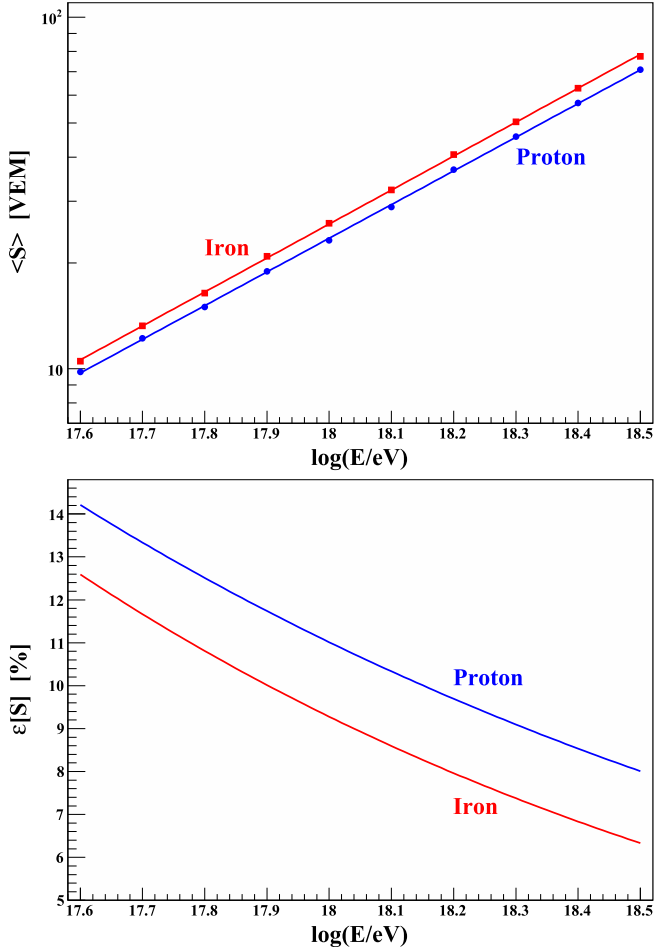\langle S\rangle(E, fe, \delta) = (1 + \delta) \times \langle S\rangle(E, fe). \tag{3}
$$

Fig. 4. Merit factor of S as a function of the logarithm of primary energy for three different values of the parameter $\delta: 0, \ 0.05$, and 0.1. The merit factor of N_μ is also shown.

factor of N_μ for comparison, which is of the order of the one corresponding to S for $\delta = 0.1$.

2.2. Analysis of the bias

The mean value of the number of muons at a given distance to the shower axis is a parameter commonly used to infer the primary mass of the cosmic rays (see for instance [48–50]), due to its large sensitivity to the nature of the primary. In this section the effects on the determination of the mean value of N_μ, introduced by the use of an energy scale dependent on composition are studied, considering a realistic physical situation. Also, a simplified case is analyzed in Appendix A for which explicit analytical expressions of the most relevant quantities discussed here can be obtained.

The calibration curve relates a parameter used as energy estimator (the signal S in this case) with the reconstructed energy. Let us denote the calibration curve as $S^{\mathcal{C}}_{cal}(E_{rec})$ where $\mathcal{C}$ indicates that this function depends on the composition of the cosmic rays.

The flux of a given primary can be written as $J_A(E) = c_A(E) J(E)$, where $J(E)$ is the total flux and $c_A(E)$ is the abundance corresponding to a primary of type A. Therefore,

$$P(A|E) = c_A(E), \tag{6}$$

$$P(E|A) = \frac{c_A(E)J(E)}{\int_0^\infty dE\, c_A(E) J(E)}, \tag{7}$$

$$P(E) = \frac{J(E)}{\int_0^\infty dE J(E)}, \tag{8}$$

where $P(A|E)$ is the probability to find a nucleus of type A given the true energy, $P(E|A)$ is the energy distribution given the primary type, and $P(E)$ is the energy distribution of all species. Note that $\sum_A c_A(E) = 1$.

The combined distribution function of the number of muons and the reconstructed energy is given by,

$$P(N_\mu, E_{rec}|E, A) = P(N_\mu, S^{\mathcal{C}}_{cal}(E_{rec})|E, A) \frac{\partial S^{\mathcal{C}}_{cal}}{\partial E_{rec}}(E_{rec}). \tag{9}$$

Therefore, the distribution function of N_μ given the primary type and the reconstructed energy is obtained from Eq. (2))

$$P(N_\mu|E_{rec}, A) = \frac{1}{M(E_{rec}, A)} \int_0^\infty dE\, c_A(E) J(E) \times P(N_\mu, S^{\mathcal{C}}_{cal}(E_{rec})|E, A),$$

$$\tag{10}$$

Fig. 3. Top panel: Mean value of S as a function of the logarithm of primary energy for proton and iron primaries. Bottom panel: Relative error on the determination of S as a function of the logarithm of primary energy for proton and iron primaries.

The standard deviation of S for both proton and iron nuclei is not modified. Note that $2 \times \delta$ corresponds to the fraction of the average $(\langle S \rangle(E, fe) + \langle S \rangle(E, pr))/2$ added to the difference between the mean value of S for iron and proton primaries, as can be seen from the following equation,

$$\langle S \rangle(E, fe, \delta) - \langle S \rangle(E, pr, \delta) = \Delta_- \langle S \rangle(E) + \delta \Delta_+ \langle S \rangle(E), \tag{4}$$

where $\Delta_\pm \langle S \rangle(E) = \langle S \rangle(E, fe) \pm \langle S \rangle(E, pr)$.

The discrimination power of a given mass sensitive parameter, q, can be assessed by the commonly used merit factor, which is defined as,

$$MF(q) = \frac{\langle q \rangle_{fe} - \langle q \rangle_{pr}}{\sqrt{Var[q]_{fe} + Var[q]_{pr}}}, \tag{5}$$

where $Var[q]_A$ is the variance of parameter q for primary type A. Fig. 4 shows the merit factor of S as a function of the logarithm of primary energy for three different values of $\delta: 0, 0.05$, and 0.1. As expected the merit factor increases with primary energy (see Fig. 3). Also, from the figure it can be seen that for $\delta = 0$ the merit factor is smaller than one in the whole energy range under consideration, indicating that the discrimination power of S is quite poor. For increasing values of δ the MF increases such that for $\delta = 0.1$ it is larger than 1.5 in the whole energy range, reaching values close to 3 for energies near $E = 10^{18.5}$ eV. The figure also shows the merit
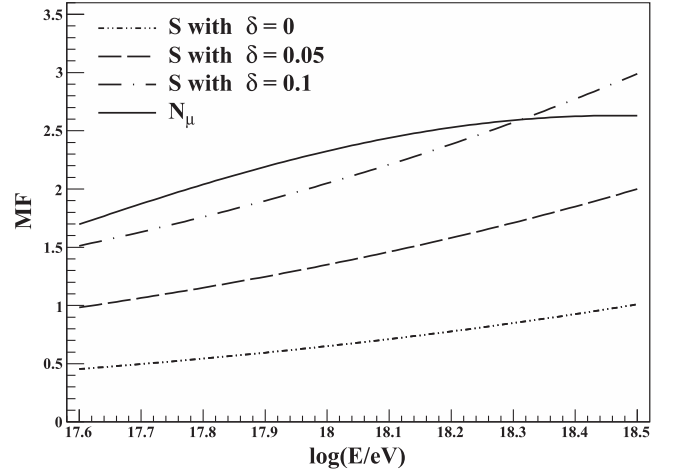
where,

$$M(E_{rec}, A) = \int_0^\infty dN_\mu \int_0^\infty dE\, c_A(E) J(E) \times P(N_\mu, S_{cal}^{\mathcal{C}}(E_{rec})|E, A) \quad (11)$$

is the normalization of the distribution function.

A power law energy spectrum is considered in all subsequent calculations. Therefore, the total flux can be written as,

$$J(E) = C\, E^{-\gamma}, \quad (12)$$

where C is a constant and γ is the spectral index.

2.2.1. Constant composition

Let us first consider the simplified case in which there are just two nuclear species, proton and iron, and that the proton abundance c_p is independent of primary energy. Assuming that the calibration curve is given by the mean value of the signal the following expression is obtained,

$$S_{cal}^{\mathcal{C}}(E_{rec}) = c_p \langle S \rangle (E_{rec}, pr) + (1 - c_p) \langle S \rangle (E_{rec}, fe). \quad (13)$$

Note that the dependence on composition of the calibration curve is given explicitly.

The signal S corresponding to iron nuclei is larger than the one for protons (see Fig. 3). Therefore, from Eq. (13) it can be seen that the reconstructed energy for iron nuclei is larger than the true one and for proton primaries is smaller. This bias in energy is translated into a bias in composition analyses when a parameter with a strong dependence on primary energy, like the number of muons at ground, is considered.

Fig. 5 shows the distribution functions of N_μ for proton and iron primaries for $E = E_{rec} = 10^{18}$ eV and for $\delta = 0$ (top panel) and $\delta = 0.1$ (bottom panel). The proton abundance considered is $c_p = 0.5$ and the spectral index is $\gamma = 3.27$, which corresponds to the experimental value obtained by The Pierre Auger Observatory in the energy range under consideration [51]. It can be seen that the distribution functions of proton and iron primaries get closer. Note that the distribution function of iron nuclei is more affected than the one corresponding to proton primaries. This is because the calibration curve tends to move the distribution function of protons to the right and the one corresponding to iron nuclei to the left, however, the energy spectrum tends to move both distributions to the left. Also, from the figure it can be seen that the modification of the distribution functions is more important for increasing values of δ, as expected.

The mean value of N_μ for a given primary type A, as a function of the reconstructed energy and for a proton abundance $c_A(E)$ can be calculated from Eq. (10),

$$\langle N_\mu \rangle (E_{rec}, A) = \frac{1}{M(E_{rec}, A)} \int_0^\infty dE \int_0^\infty dN_\mu\, N_\mu\, c_A(E)$$
$$\times J(E) P(N_\mu, S_{cal}^{\mathcal{C}}(E_{rec})|E, A), \quad (14)$$

which, by using Eq. (1), takes the following form,

$$\langle N_\mu \rangle (E_{rec}, A) = \frac{1}{M(E_{rec}, A)}$$
$$\times \int_0^\infty dE\, c_A(E) J(E) \exp\left[-\frac{(S_{cal}^{\mathcal{C}}(E_{rec}) - \langle S \rangle(E, A))^2}{2\,\sigma^2[S](E, A)} \right]$$
$$\times \left(\langle N_\mu \rangle (E, A) + \rho(E, A) \frac{\sigma[N_\mu](E, A)}{\sigma[S](E, A)} \right.$$
$$\left. \times \left(S_{cal}^{\mathcal{C}}(E_{rec}) - \langle S \rangle(E, A) \right) \right). \quad (15)$$

Note that the correlation introduces a term which is directly added to the mean value of N_μ as a function of the true energy.
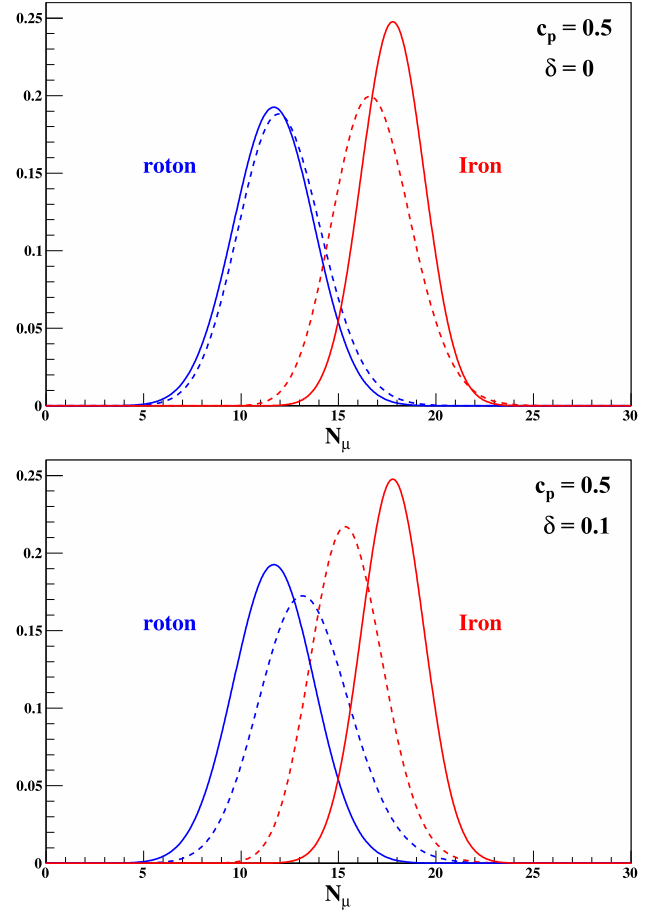

Fig. 5. Distribution functions of N_μ for proton and iron primaries of $E = E_{rec} = 10^{18}$ eV. Top panel: $\delta = 0$ and bottom panel: $\delta = 0.1$. Solid lines correspond to the true energy and dashed line to the reconstructed energy.

Therefore, from Eqs. (7), (9), and (14) it can be demonstrated that the mean value of N_μ as a function of the reconstructed energy, corresponding to a mixture of nuclei, is given by,

$$\langle N_\mu \rangle (E_{rec}) = \sum_A \langle N_\mu \rangle (E_{rec}, A)\, \omega_A(E_{rec}), \quad (16)$$

where $\omega_A(E_{rec}) = M(E_{rec}, A)/\sum_A M(E_{rec}, A)$. Note that for the ideal case in which the reconstructed energy is equal to the true energy it easy to show that $\omega_A(E_{rec}) = c_A(E_{rec})$.

Fig. 6 shows the mean value of N_μ as a function of the logarithm of primary energy for protons, iron nuclei, and a mixture of both such that $c_p = 0.5$ in the whole energy range. Also in this case, the solid lines correspond to the true energy ($E = \tilde{E}$) and the dashed lines correspond to the reconstructed energy ($E_{rec} = \bar{E}$).

From Fig. 6 it can be seen that the mean value of N_μ corresponding to each primary is affected by the dependence of the reconstructed energy on the proton abundance. In particular the mean value corresponding to iron nuclei is underestimated and the one corresponding to protons is overestimated. This effect is quite large for the case of $\delta = 0.1$. However when the mean value of the mixture is considered there is a cancelation that makes the difference between the true values and the ones corresponding to the reconstructed energy small.

In order to quantify the difference between the true value of $\langle N_\mu \rangle$ and the one obtained by using the reconstructed energy let us introduce the relative bias (see Appendix A for a simplified case in which the bias can be calculated explicitly), which is defined as,
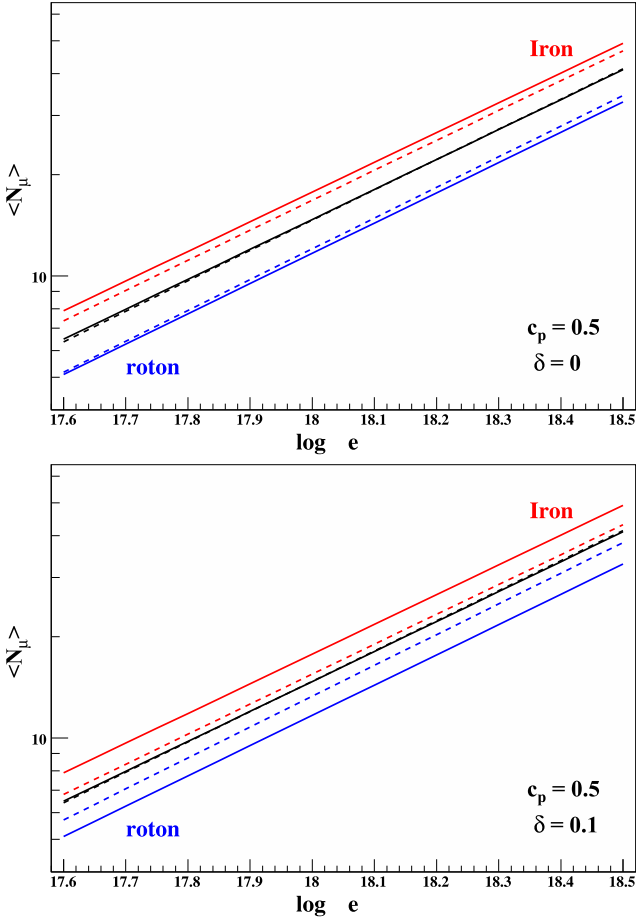
Fig. 6. Mean value of N_μ as a function of the logarithm of the energy for protons, iron nuclei, and a mixture of both primaries such that $c_p = 0.5$. Top panel: $\delta = 0$ and bottom panel: $\delta = 0.1$. Solid lines correspond to the true energy and dashed lines to the reconstructed energy.

$$R_b(\widetilde{E}) = \frac{\langle N_\mu \rangle (E_{rec} = \tilde{E})}{\langle N_\mu \rangle (E = \tilde{E})} - 1. \qquad (17)$$

Note that R_b is positive for the case in which the true value of $\langle N_\mu \rangle$ is smaller than the one obtained by using the reconstructed energy.

Fig. 7 shows the relative bias as a function of proton abundance for $\tilde{E} = 10^{18}$ eV and for $\delta = 0$ and $\delta = 0.1$. Both curves present a maximum between $c_p = 0.5$ and $c_p = 0.7$. The relative bias corresponding to $\delta = 0$ takes values between -1.5% and -0.5%, whereas the relative bias for $\delta = 0.1$ takes values between -1.9% and 0.2%. Therefore, for $\delta = 0.1$ the bias is extended in a wider range than for $\delta = 0$. In the extreme cases, $c_p = 0$ and $c_p = 1$, the bias comes only from the convolution between the spectrum and the energy uncertainty because the composition is pure in both cases. From the figure it can be seen that for $\delta = 0$ the absolute value of the relative bias is slightly larger for $c_p = 0$. This is due to the larger muon content of iron showers, which is more important than the reduction of the absolute value of the bias for iron nuclei coming from the smaller energy uncertainty (see bottom panel of Fig. 3). For the $\delta = 0.1$ case the absolute value of the relative bias for $c_p = 0$ is smaller than the one corresponding to $c_p = 1$. This is because for $\delta > 0$ the relative error of S increases for protons and decreases for iron nuclei ($\sigma[S]$ is kept constant).

Fig. 8 shows the relative bias on the determination of the mean value of N_μ as a function of the logarithm of primary energy for $\delta = 0$ (top panel) and $\delta = 0.1$ (bottom panel) and for $c_p = 0.2, 0.6$, and 0.9. The value of the spectral index used is the
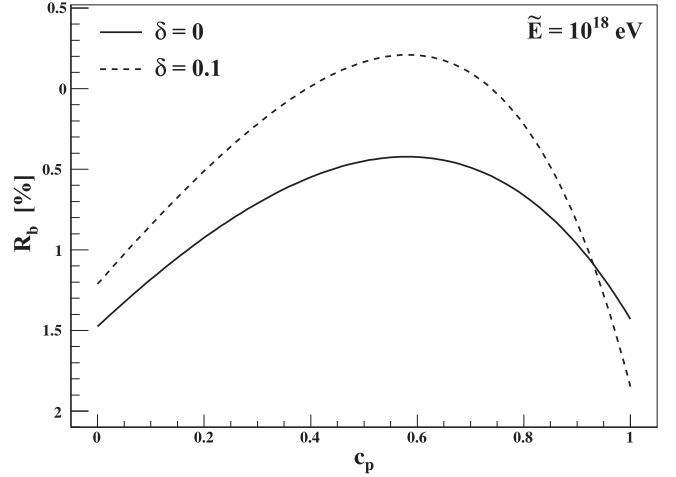

Fig. 7. Relative bias as a function of proton abundance for $\bar{E} = 10^{18}$ eV and for $\delta = 0$ and $\delta = 0.1$.
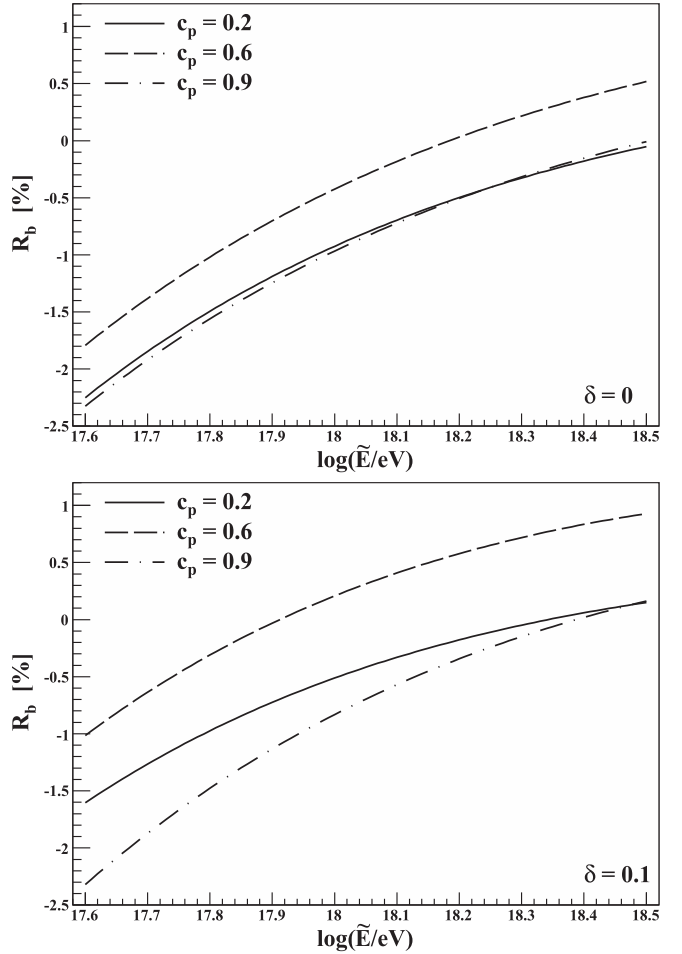

Fig. 8. Relative bias on the determination of $\langle N_\mu \rangle$ as a function of the logarithm of the energy. Top panel: $\delta = 0$ and bottom panel: $\delta = 0.1$. Three values of proton abundance are considered, $c_p = 0.2$, 0.6, and 0.9.

same as before, $\gamma = 3.27$. For both values of δ and for all values of c_p the absolute value of the relative bias is smaller than $\sim 2.8\%$ in the energy range under consideration. This value corresponds to the maximum of the module of the relative bias as a function of c_p for $\tilde{E} = 10^{17.6}$ eV.
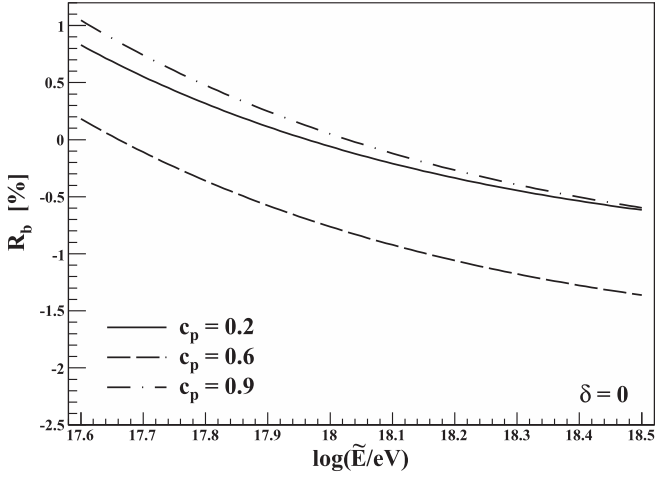
Fig. 9. Relative bias on the determination of $\langle N_\mu \rangle$ as a function of the logarithm of the energy for $\delta = 0$ and $\gamma = 0$. Three values of proton abundance are considered, $c_p = 0.2$, 0.6, and 0.9.

As mentioned before, the bias on the determination of the mean value of N_μ depends on the spectral shape of both primaries. Fig. 9 shows the relative bias as a function of the logarithm of primary energy for $\gamma = 0$ and for $\delta = 0$. Comparing this figure with the top panel of Fig. 8 it can be seen that the relative bias has a quite different shape for different values of the spectral index γ. However, its absolute value is still quite small, less than ~1.4% in this case.

For the case of $\gamma = 0$ the decrease of the relative bias with primary energy is dominated by the slower increase of the mean value of N_μ as a function of the reconstructed energy, corresponding to iron primaries, compared with the one corresponding to the true energy. This is due to the fact that as the energy increases the merit factor of S also increases (see Fig. 4), then the bias coming from the dependence of the energy on c_p is more important for increasing values of energy. The mean value of N_μ for iron primaries is more affected by this effect because the fluctuations of N_μ are smaller than the ones corresponding to protons. For the case of $\gamma = 3.27$ the increase of the relative bias with primary energy is dominated by the faster increase of the mean value of N_μ as a function of the reconstructed energy, corresponding to proton primaries, compared with the one corresponding to the true energy. In this case the fast decrease of the energy spectrum with primary energy tends to move the mean value of N_μ towards smaller values than the true ones but this effect is gradually smaller as the energy increases because the fluctuations of S decrease with primary energy (see Fig. 3). As a consequence, the mean value of N_μ as a function of the reconstructed energy corresponding to iron primaries is smaller than the one corresponding to $\gamma = 0$ but the difference with the true value as a function of primary energy is almost constant. For proton primaries the mean value of N_μ is also smaller compared with the one corresponding to $\gamma = 0$ also due to the fast decrease of the energy spectrum. As for the case of iron nuclei this effect is less important for increasing energy making the mean value of N_μ to increase faster than the true one.

2.2.2. Varying composition

Let us consider the case in which the composition profile depends on primary energy. For that purpose the following shape for the proton abundance is assumed,

$$c_p(E) = \frac{1 + \tanh(a \, \log(E/E_0))}{2}. \tag{18}$$
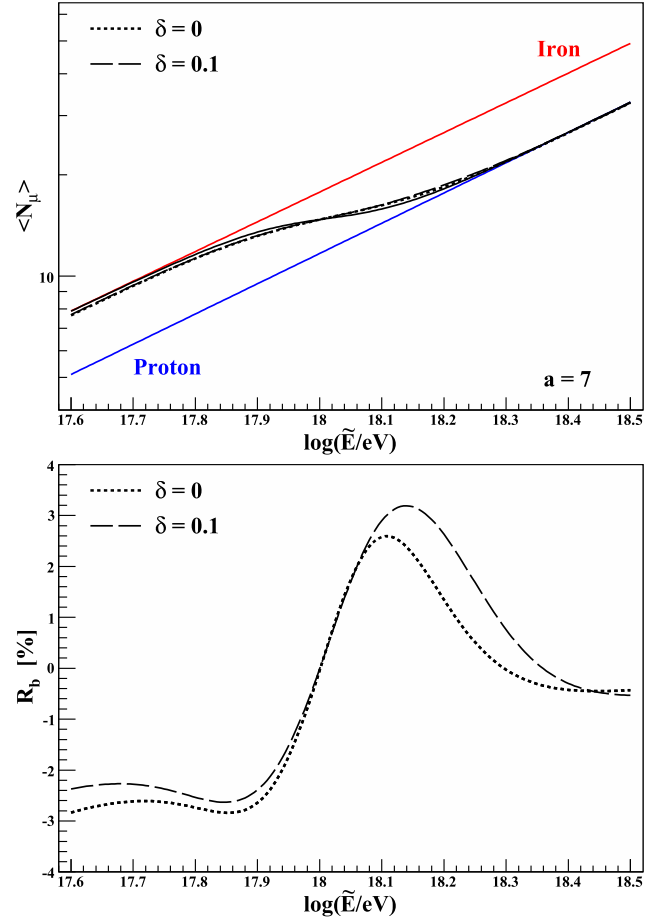

Fig. 10. Top panel: Mean value of N_μ as a function of the logarithm of primary energy. Bottom panel: Relative bias as a function of the logarithm of primary energy. The dotted and dashed lines correspond to $\delta = 0$ and $\delta = 0.1$, respectively. The parameters corresponding to the composition profile are: $E_0 = 10^{18}$ eV and $a = 7$ (see Eq. (18)).

It represents a transition from iron nuclei at low energies to protons at high energies. The transition is given at an energy E_0 and the speed at which this transition takes place is controlled by the parameter a. The larger the values of a the faster the transition from iron nuclei to protons.

The top panel of Fig. 10 shows the mean value of the number of muons as a function of the logarithm of primary energy for $E_0 = 10^{18}$ eV and $a = 7$. The calibration curve assumed for the calculation is given by Eq. (13) but in this case the proton abundance is a function of energy (given by Eq. (18)). When the reconstructed energy is considered (dashed and dotted lines) an energy dependent bias appears. For both values of δ considered ($\delta = 0$ and $\delta = 0.1$) the transition from iron nuclei to protons becomes slower than in the real composition profile. The bottom panel of Fig. 10 shows the corresponding relative bias as a function of energy for $\delta = 0$ and $\delta = 0.1$. It can be seen that in both cases the relative bias takes values between ~−3% and ~3.2%. Note that for $\delta = 0.1$ the relative bias expands over a slightly larger region than for $\delta = 0$ but the difference is small.

3. Conclusions

In this work we have studied the importance of a composition dependent energy scale on composition analyses. The method pursued dwells on a combined distribution function of the mass and energy estimator parameters which allows to analytically perform all further analyses and their physical interpretation. In this paper we have shown the strength of this approach which might be

applied to different experimental scenarios with appropriate distribution function. This approach allows a clear insight in the impact of different mass composition mixing, which is of paramount importance to understand the cosmic ray spectrum, in particular in composition changing regions.

We have applied the method developed to AMIGA in order to exemplify these effects in a realistic experimental context. We have taken the number of muons and the signal in the water-Cherenkov detectors, both evaluated at 600 m from the shower axis, as the mass sensitive and energy estimator parameters, respectively. We have found that the distribution functions of the number of muons for proton and iron primaries can be modified when an energy calibration dependent on composition is used to reconstruct the energy of the events. However, the relative bias on the determination of the mean value of the number of muons is quite small, of the order of a few % in the whole energy range under consideration. This is true even for energy estimators with merit factors of the order of the one corresponding to the number of muons. We have obtained the same upper limit on the relative bias for the two physical situations that we have considered: a constant proton abundance as a function of primary energy and a smooth transition from iron to proton primaries at $E = 10^{18}$ eV.

It is worth mentioning that the impact of the use of an energy scale dependent on composition in composition analyses has to be analyzed in detail in each particular case. The reason for that is that the effects introduced by this practice depend on the parameter sensitive to the primary mass under consideration, on the type of detectors used to observe the air showers, and on the methods used to reconstruct the shower parameters.

Acknowledgments

Appendix A. A simplified case

In the simplified physical situation treated here it is assumed that the fluctuations of the parameter used to reconstruct the primary energy are negligible, i.e. $\sigma[S](E,A) = 0$ for $A = pr$ and fe. Considering that the energy calibration is given by the mean value of the signal, it is possible to obtain the true energy E of each primary as a function of the reconstructed energy from the following expression,

$$\langle S \rangle(E,A) = c_p \langle S \rangle(E_{rec}, pr) + (1 - c_p)\langle S \rangle(E_{rec}, fe). \tag{A.1}$$

Here a binary mixture of protons and iron nuclei and a constant proton abundance are assumed.

The mean value of the number of muons is obtained, in this case, following a similar procedure to the one described in Section 2.2,

$$\langle N_\mu \rangle(E_{rec}) = \left(c_p \langle N_\mu \rangle(E(E_{rec}, pr), pr) J(E(E_{rec}, pr)) \right.$$
$$\times \frac{\partial E}{\partial E_{rec}}(E_{rec}, pr) + (1 - c_p)$$
$$\times \langle N_\mu \rangle(E(E_{rec}, fe), fe) J(E(E_{rec}, fe)) \times \frac{\partial E}{\partial E_{rec}}(E_{rec}, fe) \right)$$
$$\times \left(c_p J(E(E_{rec}, pr)) \times \frac{\partial E}{\partial E_{rec}}(E_{rec}, pr) + (1 - c_p)J(E(E_{rec}, fe)) \right.$$
$$\left. \times \frac{\partial E}{\partial E_{rec}}(E_{rec}, fe) \right)^{-1}. \tag{A.2}$$

The mean values of parameters N_μ and S have an almost linear dependence on primary energy. Then, in order to further simplify the calculation let us assume an exact linear dependence on primary energy of the mean value of both parameters,

$$\langle N_\mu \rangle(E,A) = N_{\mu,0}^A \left(\frac{E}{E_0} \right), \tag{A.3}$$

$$\langle S \rangle(E,A) = S_0^A \left(\frac{E}{E_0} \right), \tag{A.4}$$

where E_0 is a reference energy. Therefore, the mean value of N_μ as a function of the true energy is given by,

$$\langle N_\mu \rangle(E) = \left(c_p N_{\mu,0}^{pr} + (1 - c_p) N_{\mu,0}^{fe} \right) \left(\frac{E}{E_0} \right). \tag{A.5}$$

By using Eqs. (A.1)–(A.5) the relative bias on the mean value of the number of muons as a function of the reconstructed energy can be written as,

$$R_b = \frac{(R_\mu - R_S)(R_S^{\gamma-2} - 1) c_p (1 - c_p)}{(c_p + R_\mu(1 - c_p))\left(c_p + R_S^{\gamma-1}(1 - c_p)\right)}, \tag{A.6}$$

where,

$$R_\mu = \frac{N_{\mu,0}^{fe}}{N_{\mu,0}^{pr}}, \tag{A.7}$$

$$R_S = \frac{S_0^{fe}}{S_0^{pr}}. \tag{A.8}$$

Here a power law energy spectrum of the form $J(E) = C E^{-\gamma}$ is assumed.

From Eq. (A.6) it can be seen that the relative bias is independent on primary energy. Also, when the composition is pure, the cosmic rays are only protons or iron nuclei ($c_p = 1$ or $c_p = 0$), the relative bias is zero, as expected. Moreover, the bias also disappears when $R_S = 1$, $R_\mu = R_S$, or $\gamma = 2$. Fig. A.11 shows the relative bias as a function of the proton abundance for different values of γ, starting from $\gamma = 0$ up to $\gamma = 3.3$ in steps of $\Delta\gamma = 0.1$. The values $R_S = 1.1$ and $R_\mu = 1.5$ are used to make the plot, which correspond to the ratios between the mean values of each parameter (N_μ and S) for proton and iron at $E = 10^{18}$ eV.

From Fig. A.11 it can be seen that the relative bias is an increasing function of γ, it goes from negative values at $\gamma = 0$ to positive values for $\gamma > 2$. This behavior can be understood from the fact that for a given value of the reconstructed energy proton events come
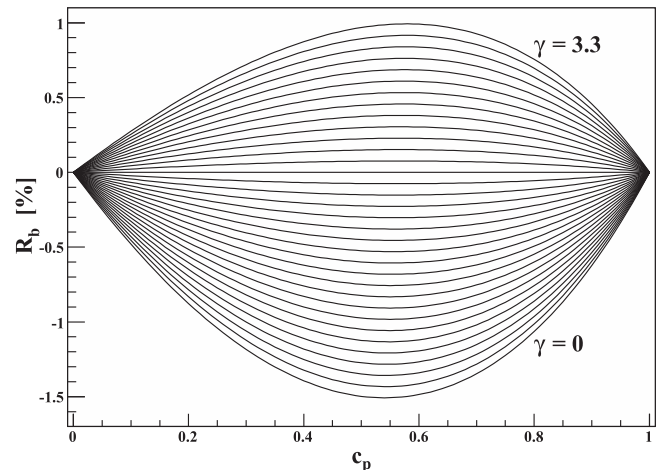

Fig. A.11. Relative bias as a function of proton abundance for different values of the spectral index starting from $\gamma = 0$ up to $\gamma = 3.3$ in steps of $\Delta\gamma = 0.1$.

from larger values of the true energy but iron events come from smaller values, therefore, for a power law energy spectrum the iron events have a larger weight, which increases with γ moving the mean value towards the one corresponding to iron nuclei. In this way, after increasing γ sufficiently the relative bias becomes positive.

For every $\gamma \neq 2$, the relative bias has an extreme point placed at an intermediate value of the proton abundance. This extreme value is a maximum if $\gamma > 2$ and it is a minimum if $\gamma < 2$. The expression for the proton abundance corresponding to the extreme point can be obtained from Eq. (A.6), which is given by,

$$c_p^{ext} = \frac{R_\mu R_S^{\gamma-1} - \sqrt{R_\mu R_S^{\gamma-1}}}{R_\mu R_S^{\gamma-1} - 1}, \tag{A.9}$$

which is valid for $R_S \neq 1$, $R_\mu \neq R_S$, and $\gamma \neq 2$. As can be seen from figure A.11, c_p^{ext} varies very slowly with γ, in fact it goes from ~ 0.54 at $\gamma = 0$ to ~ 0.58 at $\gamma = 3.3$.

References

[1] G. Kulikov, G. Khristiansen, J. Exp. Theor. Phys. 35 (1958) 635.
[2] M. Aglietta et al., Astropart. Phys. 20 (2004) 641.
[3] T. Antoni et al., Astropart. Phys. 24 (2005) 1.
[4] W. Apel et al., Astropart. Phys. 31 (2009) 86.
[5] M. Amenomori et al., Adv. Space Res. 47 (2011) 629.
[6] T. Abu-Zayyad et al., Astrophys. J. 557 (2001) 686.
[7] M. Ave et al., in: Proc. 27th ICRC (Hamburg), 2001, p. 381.
[8] M. Pravdin et al., in: Proc. 28th ICRC (Tuskuba), 2003, p. 389.
[9] R. Abbasi et al., Phys. Rev. Lett. 100 (2008) 101101.
[10] R. Abbasi et al., Astropart. Phys. 32 (2009) 53.
[11] J. Abraham et al., Phys. Rev. Lett. 101 (2008) 061101.
[12] T. Abu-Zayyad et al., Astrophys. J. Lett. 768 (2013) L1.
[13] W. Apel et al., Phys. Rev. Lett. 107 (2011) 171104.
[14] R. Baltrusaitis et al., Nucl. Instrum. Methods Phys. Res. A 240 (1985) 410.
[15] T. Abu-Zayyad et al., Nucl. Instrum. Methods Phys. Res. A 450 (2000) 253.
[16] J. Abraham et al., Nucl. Instrum. Methods Phys. Res. A 620 (2010) 227.
[17] H. Tokuno et al., Nucl. Instrum. Methods Phys. Res. A 676 (2012) 54.
[18] A. Letessier-Selvon, T. Stanev, Rev. Mod. Phys. 83 (2011) 907.
[19] K. Kotera, A. Olinto, Annu. Rev. Astron. Astrophys. 49 (2011) 119.
[20] K.H. Kampert, M. Unger, Astropart. Phys. 35 (2012) 660.
[21] G. Medina-Tanco for the Pierre Auger Collaboration, in: Proceedings of 30th ICRC, Mérida, México, vol. 5, 2007, p. 1101.
[22] K. Kampert, Braz. J. Phys. 43 (2013) 375. <arXiv:1305.2363>.
[23] A.D. Supanitsky, A. Etchegoyen, G. Medina-Tanco, Astropart. Phys. 31 (2009) 116.
[24] C. Song et al., Astropart. Phys. 14 (2000) 7.
[25] M. Tueros for the Pierre Auger Collaboration, in: Proceedings of 33rd ICRC, Rio de Janeiro, Brazil, 2013, <arXiv:1307.5059>.
[26] T. Pierog, EPJ Web Conf. 53 (2013) 01004.
[27] S. Ostapchenko, EPJ Web Conf. 52 (2013) 02001.
[28] T. Pierog, EPJ Web Conf. 52 (2013) 03001.
[29] T. Csörgö et al., Prog. Theor. Phys. Suppl. 193 (2012) 180.
[30] V. Khachatryan et al., Phys. Rev. Lett. 105 (2010) 022002.
[31] K. Aamodt et al., Eur. Phys. J. C 68 (2010) 345.
[32] M. Chojnacki et al., J. Phys. G 38 (2011) 124074.
[33] S. Chatrchyan et al., Eur. Phys. J. C 72 (2012) 2164.
[34] G. Ros, A.D. Supanitsky, G.A. Medina-Tanco, L. del Peral, J.C. DOlivo, M.D. Rodríguez-Frías, Astropart. Phys. 35 (2011) 140.
[35] A. Etchegoyen for the Pierre Auger Collaboration, in; Proceedings of 30th ICRC, Mérida, México, vol. 5, 2007, p. 1191.
[36] A.D. Supanitsky, A. Etchegoyen, G. Medina-Tanco, I. Allekotte, M. Gómez Berisso, M.C. Medina, Astropart. Phys. 29 (2008) 461.
[37] J. Abraham et al., Nucl. Instrum. Methods Phys. Res. A 523 (2004) 50.
[38] M. Ave et al., Astropart. Phys. 19 (2003) 61.
[39] J. Abraham et al., Astropart. Phys. 29 (2008) 243.
[40] T. Dova et al., Astropart. Phys. 21 (2004) 597.
[41] G. Rubtsov et al., in: Proc. 33rd ICRC, Rio de Janeiro, Brazil, 2013, #0149.
[42] S. Sciutto, AIRES users manual and reference guide, 2002. <http://www2.fisica.unlp.edu.ar/auger/aires/>.
[43] S. Ostapchenko, Nucl. Phys. B. Proc. Suppl. 151 (2006) 143.
[44] N. Hayashida et al., J. Phys. G: Nucl. Part. Phys. 21 (1995) 1101.
[45] X. Bertou et al., Nucl. Instrum. Methods Phys. Res. A568 (2006) 839.
[46] J.C. Arteaga-Velazquez et al., in: Proceedings of 33rd ICRC, Rio de Janeiro, Brazil, 2013. Available from: <arXiv:1308.3202>.
[47] G. Farrar for The Pierre Auger Collaboration, in: Proc. 33rd ICRC, Rio de Janeiro, Brazil, 2013. Available from: <arXiv:1307.5059>.
[48] M. Glasmacher et al., Astropart. Phys. 12 (1999) 1.
[49] K. Shinozaki et al., in: Proceedings of 29th ICRC 7, 2005, p. 151.
[50] A. Glushkov, A. Sabourov, 2013. Available from: <arXiv:1310.0561>.
[51] D. Ravignani for the Pierre Auger Collaboration, in: Proceedings of 33rd ICRC, Rio de Janeiro, Brazil, 2013. Available from: <arXiv:1307.5059>.